Universal Quality Assurance Method for Resistance Spot Welding Based on Dynamic Resistance

Dynamic-resistance-based universal quality assurance method provides the maximum nugget size

BY A. G. LIVSHITS

ABSTRACT. Welding of mild steel is one of the most common processes in spot welding. Numerous methods for ensuring high-quality welds are based on dynamic resistance. However, in general, these methods are only useful over a relatively narrow range of welding parameters. This article presents a universal quality assurance method based on dynamic resistance that is valid over a wide range of welding time, welding current, electrode force and electrode tip geometry (up to and including complete tip mushrooming). This method was constructed on the basis of models describing current density redistribution at the faying surface during the welding process. Validation of the method has been confirmed experimentally. The comparison of results shows that the method provides the maximum nugget size.

Introduction

Quality assurance methods based on dynamic resistance are used in the welding of mild steel. An advantage of dynamic resistance methods is that they do not require the use of complicated sensors for measurement of relevant electrical parameters, and they permit straightforward implementation of real-time systems for controlling the quality of each welded spot. The goal of such real-time control systems is the determination of the moment when the nugget reaches its optimal size so that the welding current can be terminated precisely.

Let us denote the resistance between electrode tips by R_d. A typical curve of time variation in resistance $R_d(t)$ for welding uncoated mild steel is presented in Fig. 1.

The physical processes taking place in each of designated zones are commonly known.

The reduction of the resistance, at the expense of increasing the number of contact points inside the physical contact area and of film breakdown on the contact surface, occurs in Zone 1. At the end of Zone 1 the minimum resistance R_{min} is achieved, indicating good contact between the workpieces and between the workpieces and electrodes.

Subsequent increase in the resistance R_d (Zone 2) is associated, for the most part, with increase of specific resistance of the material, due to its heating.

Melting results in the indentation of the electrode tips into the material, which, in turn, causes a reduction of the current path. As the nugget size increases, an expansion of the contact area occurs. In this manner, the zone of resistance R_d growth is replaced by the zone of its drop (Zone 3). Maximum resistance R_{max} is achieved at the end of Zone 2. The further increase of the nugget size in Zone 3 is accompanied by the resistance R_d decreasing to the value R_{lim}, when the optimal dimension of the nugget is achieved.

Though mild steels have a wide weldable range, conventional quality assurance methods employing dynamic resistance are suitable over relatively narrow ranges of welding parameters.

This is mainly due to the fact that these methods consider the resistance variation as a time function, ignoring the effect of heat generation, heat loss to the electrodes, and electrode geometry on the dynamic resistance variation.

In this work, a universal method for assuring the quality and consistency of resistance spot welds in uncoated steel sheet is proposed. The method is valid over a wide range of welding time, welding current, electrode force and electrode tip geometry. The method was constructed on the basis of a model describing current density redistribution at the faying surface during the welding process and, in most cases, does not require specific information about welding conditions. In this article, methods of sensing or controlling weld parameters are not presented. Reference 1 describes methods of measuring and monitoring dynamic electrical properties and is a good source.

KEY WORDS

Resistance Spot Weld
Quality Assurance
Dynamic Resistance
Adaptive Controls
Real Time Control
Control Algorithm
Uncoated Steel
Nugget Size
Electrode Geometry
Expulsion

Model Structure

The model is based on the physical events described that contribute to the dynamics of resistance variation. The resistance between electrode tips is modeled as a linear active resistance, *i.e.*, the resistance can be obtained by dividing the voltage by the current. It is, therefore, convenient to model the dynamics of this resistance variation to the dynamics of current change, assuming that the voltage is constant. This condition refers to the design procedure and enables one to describe changes in conductivity distribution. It does not limit the real change in either voltage or current during the welding process. This article will show that the electrode geometry is a substantial factor affecting welding current density distribution. For this reason, two principal cases concerning spherical-end electrodes and flat-end electrodes will be studied.

The First Approximation Model

Let us discuss the first approximation model in which the increase of contact area at welding is ignored. The radius of contact is invariable and is equal to the initial radius of physical contact r_{ci}.

A. G. LIVSHITS is with Welding Technologies, Blue Bell, Pa.

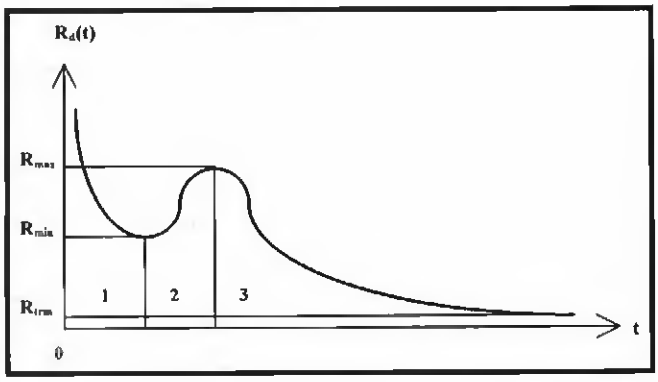

Fig. 1 — Typical dynamic resistance curve.

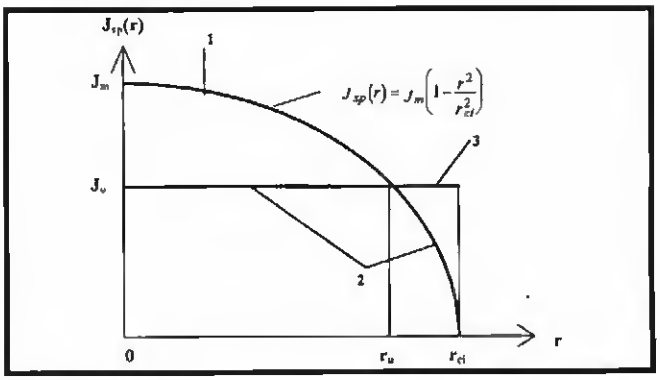

Fig. 2 — Spherical-end electrode. Schematic illustration of current density distribution at the faying surface: 1, 2, 3 — current density distribution at the end of Zone 1, Zone 2, and Zone 3, respectively.

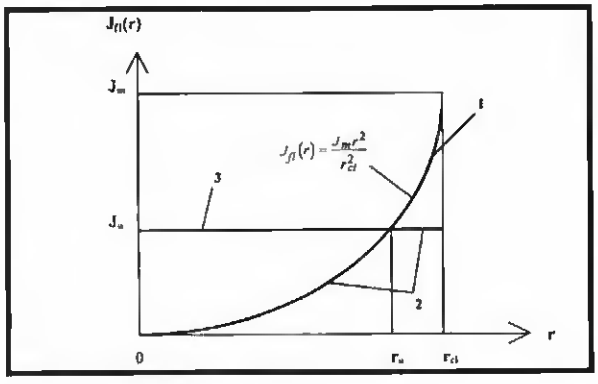

Fig. 3 — Flat-end electrode. Schematic illustration of current density distribution at the faying surface (preliminary): 1, 2, 3 — current density distribution at the end of Zone 1, Zone 2, and Zone 3, respectively.

Spherical-End Electrode

Figure 2 presents the curve of current density distribution $J_{sp}(r)$ at the faying surface at the moment the minimum on the dynamic resistance curve is reached. At this moment, the contact is determined, on the whole, by the number of contact points. Such a distribution at the faying surface reflects both the geometry of contacting elements and the pressure distribution on all the surfaces at the moment of film breakdown, as well as formation of good metallic contact between the workpieces and between the workpieces and electrodes. As the current flows, the temperature of the workpieces rises. The most intensive heat, accompanied hy a resistance increase, will be observed in a zone with maximal current density, *i.e.*, at the center of the weldment. As a result, a redistribution of current density takes place. That is precisely why the current density begins to decrease in a zone with maximal temperature and corresponds to the replacement of the sections with greater current density values, heginning with maximum value J_m, at the sections with the smaller current density value J_u.

The process of replacing sections having greater current density with sections having smaller density J_u will take place until the radius r_u is attained, which corresponds to the maximum on the dynamic resistance curve. Subsequently, at radii from r_u to r_{ci}, the sections with smaller current density are replaced by sections with greater density corresponding to the reductiun of resistance in Zone 3 on the dynamic resistance curve. It is obvious that, in Zone 1 and Zone 2 of the dynamic resistance curve, the current density distribution shape changes significantly. Nakata's research (Ref. 2) showed that for the spherical-end electrode, the value R_d is inversely proportional to the contact area soon after achieving a maximum on the dynamic resistance curve. It can be proven that such relationship between R_d and the contact area takes place if the contact area grows, but the current density distribution shape does not change ("frozen" shape). It can be concluded from literature that, at the late stages of welding process, the current density distribution shape at the faying surface becomes smoother and flatter. Most likely, the "frozen" shape corresponds to the current that is homogeneously distributed over the whole area of contact. Therefore, the homogeneous current distribution with density J_u on the section of radius r_{ci} corresponds to the welding termination.

The proposed description of current density redistribution in the process of nugget formation not only explains the behavior of the dynamic resistance curve, but also permits the prediction of variation under different welding conditions. For example, since current density J_u decreases with the growth of heat intensity, the maximum on the resistance curve will be weakly manifested by small currents. Conversely, at increased welding current levels, the maximum will be manifested strongly. The increase of electrode force results in J_m value magnification and hence in a reduction of maximum value on the dynamic resistance curve.

The model is intended for effective implementation of an adaptive control system. Therefore, it is necessary to derive numerical relationships which allow us to determine the algorithm of the control system functioning. As mentioned above, to model the dynamics of resistance, it is necessary to describe the dynamics of current change. For this purpose, we will approximate the surface distribution of current density $J_{sp}(r)$. On one hand, the approximation should be close enough to the real one, *i.e.*, such welding parameters as welding current, electrode force, electrode tip geometry and thickness of workpieces should be taken into consideration. On the other hand, the moment of the current termination should be determined only on the basis of the dynamic resistance curve, *i.e.*, direct information about the same welding parameters cannot be used. The surface distribution of current density $J_{sp}(r)$ is approximated in Fig. 2 by a parabola. It will be shown later that such an approximation allows us to derive a mathematical description that does not require the information about parameters of the parabola to determine the moment of the current termination. It also means that direct information about welding parameters is not required.

$$J_{sp}(r) = J_m\left(1-\frac{r^2}{r_{ci}^2}\right) \qquad (1)$$

Let us calculate the current I_{Rmin}, pass-

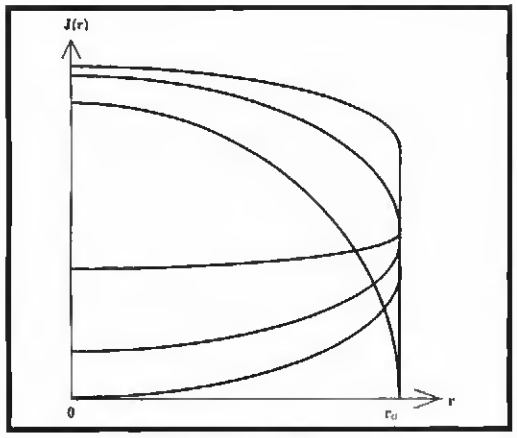

Fig. 4 — Different electrode geometry. Schematic illustration of current density distribution at the faying surface at the end of Zone 1.

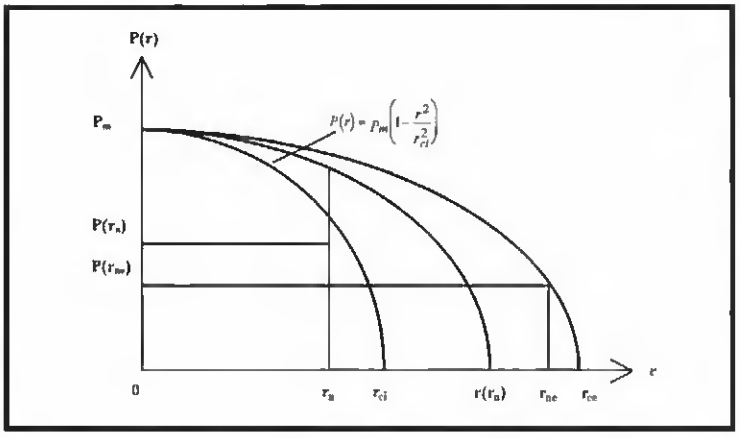

Fig. 5 — Spherical-end electrode. Schematic illustration of pressure distribution at the faying surface.

ing through the whole contact area at the moment when the minimum on the dynamic resistance curve is reached. To calculate the surface integral, we have to take into consideration the surface current density distribution 1. As a result, we obtain:

$$I_{R\min} = 2\pi \int_0^{r_{ci}} r J_m \left(1 - \frac{r^2}{r_{ci}^2}\right) dr = \frac{\pi J_m r_{ci}^2}{2} . \quad (2)$$

The current I_{Rmax}, passing through the whole contact area at the moment when the resistance reaches its maximum, is determined by the equation:

$$I_{R\max} = 2\pi \int_0^{r_u} r J_u \, dr + 2\pi \int_{r_u}^{r_{ci}} r J_m \left(1 - \frac{r^2}{r_{ci}^2}\right) dr = \frac{\pi J_m r_{ci}^2}{2} \left[1 - \left(1 - \frac{J_u}{J_m}\right)^2\right]. \quad (3)$$

The first surface integral defines the current, passing through the circle with radius r_u. The current with the surface density J_m is homogeneously distributed over the whole area of the circle. The second surface integral defines the current, passing through the coil with internal radius r_u and external radius r_{ci}. To calculate the second integral, the surface current density distribution 1 was taken into account.

Equation 3 is obtained taking into account the equation:

$$r_u^2 = \left(1 - \frac{J_u}{J_m}\right) r_{ci}^2 . \quad (4)$$

As previously mentioned, at the late stages of the welding process the current is homogeneously distributed over the whole contact area. In such instances, the welding current at the moment of the current termination I_{trm} is defined by the equation:

$$I_{trm} = 2\pi \int_0^{r_{ci}} r J_u \, dr = \pi J_u r_{ci}^2 . \quad (5)$$

The surface integral defines the current, passing through the circle with radius r_{ci}.

Since the weld joint is considered to be a linear active resistance, dividing Equation 3 by Equation 2 and Equation 5 by Equation 2, we obtain:

$$J_{sp}(r) = J_m \left(1 - \frac{r^2}{r_{ci}^2}\right) \quad (1)$$

and

$$\frac{I_{trm}}{I_{R\min}} = \frac{R_{\min}}{R_{trm}} = 2\frac{J_u}{J_m} . \quad (7)$$

Excluding the parameter J_u/J_m from Equations 6 and 7, we obtain:

$$R_{trm} = \frac{R_{\min}}{2\left(1 - \sqrt{1 - \frac{R_{\min}}{R_{\max}}}\right)} . \quad (8)$$

Equation 8 describes the desired algorithm of an adaptive control system functioning within the scope of the first approximation model.

Since time is not included in Equation 8, it is important that resistance R_{trm} is calculated based on the values of resistances R_{min} and R_{max} in typical points of the dynamic resistance curve. The model should adequately describe current density distribution just in these points; otherwise, we have no right to expect satisfactory results. The adequacy of describing the current distribution at other points is of no importance.

Flat-End Electrode

Let us similarly discuss the current density distribution in the case of the flat-end electrode. We will consider the same three points. The current density distribution corresponding to the minimal resistance is shown in Fig. 3 and reflects both the geometry of contacting elements and the pressure distribution on all the surfaces at the moment of film breakdown, and a formation of good metallic contact between the workpieces and between the workpieces and electrodes.

Let us approximate the curve of current density distribution $J_{fl}(r)$ in Fig. 3 by Parabola 9 in the same manner as we did in the case of the spherical-end electrode. Whether or not this distribution is close to the real one will be discussed later.

$$J_{fl}(r) = \frac{J_m r^2}{r_{ci}^2} \quad (9)$$

The welding process in Zone 2 of the dynamic resistance curve is characterized by a resistance value increase at the expense of metal heating and melting in the zone of maximal current density. Within the scope of our model, this corresponds to the replacement of the sections with greater current density value, beginning with J_m, by the sections with smaller current density value J_u. At the moment when the resistance reaches its maximum, the zone of relatively cool metal will be reduced to a radius r_u. After that, the replacement of the sections with

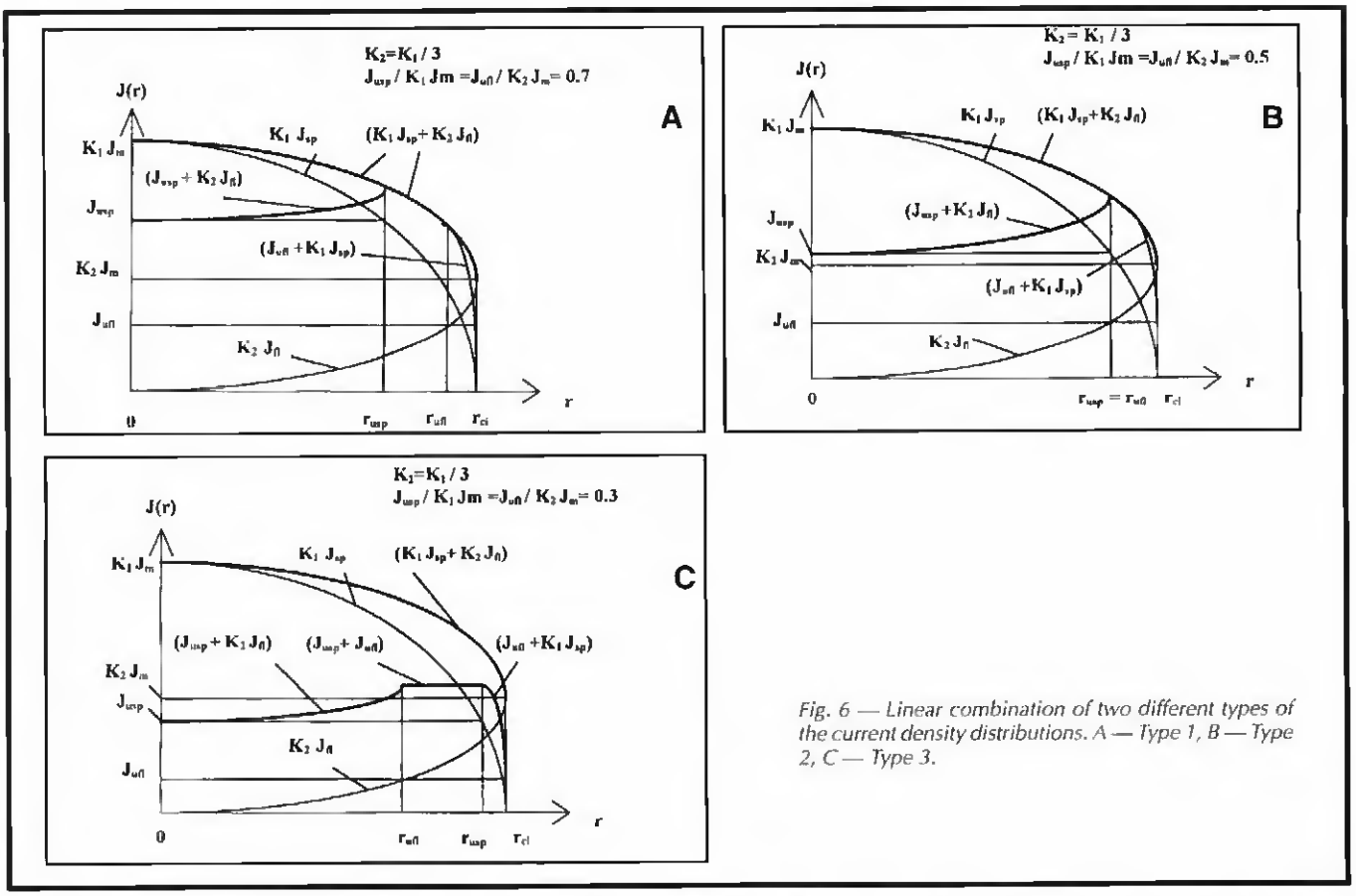

Fig. 6 — Linear combination of two different types of the current density distributions. A — Type 1, B — Type 2, C — Type 3.

relatively small current density by the sections with a relatively great one will hegin, which conforms to the resistance decreasing in Zone 3. The homogeneously distributed current with density J_u on the radius section r_{ci} corresponds to the current termination.

As in the case of the spherical-end electrode, note the equations for the currents I_{Rmin}, I_{Rmax} and I_{Rtrm} at the indicated moments, namely, Equations 10, 11, and 12, respectively.

$$I_{R\min} = 2\pi \int_0^{r_{ci}} \frac{J_m r^2}{r_{ci}^2}\, rdr = \frac{\pi J_m r_{ci}^2}{2} \quad (10)$$

$$I_{R\max} = 2\pi \int_0^{r_u} \frac{J_m r^2}{r_{ci}^2}\, rdr + 2\pi \int_{r_u}^{r_{ci}} J_u\, rdr$$

$$= \frac{\pi J_m r_{ci}^2}{2}\left[1-\left(1-\frac{J_u}{J_m}\right)^2\right] \quad (11)$$

$$I_{trm} = 2\pi \int_0^{r_{ci}} J_u\, rdr = \pi J_u r_{ci}^2 \quad (12)$$

The right sides of the Equations 10, 11, and 12 are the same as the right sides of Equations 2, 3, and 5, respectively. Thus the resistance R_{trm} is also determined by Equation 8 for the case of a flat-end electrode.

It should be emphasized again that the current density distribution is considered only at the three above mentioned moments, so the adequacy of describing the current distribution at other points is of no importance.

The comparison of the structures of Equations 1 and 9, 2 and 10, 3 and 11, S and 12 enables one to draw an important conclusion that the same result will take place, not only in the cases of current density distributions 1 and 9, but also in the case of their linear combination (Appendix):

$$J(r) = K_1 J_{sp}(r) + K_2 J_{fl}(r), \quad (13)$$

where K_1 and K_2 are positive constants.

Equation 13 was derived by taking into consideration two assumptions as noted below:

1) J_m for the spherical-end electrode is equal to J_m for the flat-end electrode;

2) r_{ci} for the spherical-end electrode is equal to r_{ci} for the flat-end electrode.

Equation 13 describes a wide spectrum of current density distributions. Some of them are shown in Fig. 4 and take place for different kinds of electrode geometry. The curve that is closest to a real distribution can be chosen. This may explain why no previous researchers of the dynamic resistance method considered electrode geometry as a factor influencing the moment of current termination (Refs. 6–11).

Some remarks on the first approximation model to be noted:

1) The model describes the resistance R_d as a function of the welding condition but not as a time function. The resistance R_{trm} depends neither on the dynamics of heat generation nor on heat loss to the electrodes.

2) Within the scope of the model the values of J_u, J_m, and r_{ci} together with the electrode geometry reflect the welding conditions. The model structure is such that the resistance R_{trm} depends neither on the electrode geometry nor on the parameters J_u, J_m, and r_{ci}; so we can expect that the model will he applicable in a relatively wide range of variations of the welding conditions.

3) The model enables one to match resistance R_{trm} with the initial diameter of physical contact, but does not connect it with the nugget diameter.

4) The model describes the current density distrihution ignoring an essential factor, the increase of contact area during the welding process.

To allow for the above listed facts, consider the pressure distribution at the faying surface. This, together with the

current density distribution, is a subject of consideration for the second approximation model.

Second Approximatinn Model

Spherical-End Electrode

Similarly to the current density distribution, let us specify the pressure distribution P(r) at the end of Zone 1 of the dynamic resistance curve (Fig. 5):

$$P(r) = P_m\left(1-\frac{r^2}{r_{ci}^2}\right). \quad (14)$$

Invariable electrode force F is determined by the equation:

$$F = 2\pi\int_0^{r_{ci}} P(r)\,rdr = \frac{\pi P_m r_{ci}^2}{2}. \quad (15)$$

With the appearance of a melted nugget of radius r_n with homogeneously distrihuted pressure $P(r_n)$ inside it, the increase of the radius of contact $r(r_n)$ will take place. In this case, the electrode force F will be expressed by equations:

$$F = 2\pi p_m\int_{r_n}^{r(r_n)}\left(1-\frac{r^2}{r^2(r_n)}\right)rdr + 2\pi P(r_n)\int_0^{r_n} rdr \quad (16)$$

and

$$F = pP_m\left[\frac{r^2(r_n)}{2}-r_n^2\left(1-\frac{r_n^2}{2r^2(r_n)}\right)\right] + pP(r)r_n^2 \quad (17)$$

Expulsion that takes place when the nugget radius r_n reaches such a value r_{ne}, when the condition in Equation 18 is realized, corresponds to the current termination.

$$P_m\left(1-\frac{r_{ne}^2}{r_{ce}^2}\right) = P(r_{ne}) \quad (18)$$

The radius of contact $r(r_n)$, obtained at this moment, is designated as r_{ce}.

The substitution of Equation 18 into Equation 17 will result in:

$$F = \frac{\pi P_m r_{ce}^2}{2}\left(1-\frac{r_{ne}^4}{r_{ce}^4}\right). \quad (19)$$

Dividing Equation 19 by Equation 15 we obtain:

$$\frac{r_{ci}^2}{r_{ce}^2} = 1-\frac{r_{ne}^4}{r_{ce}^4}. \quad (20)$$

Equation 20 defines the connection between the radii of contact at the beginning of the welding and at the moment of expulsion.

Flat-End Electrode

In the case of a flat-end electrode, the expulsion condition may be expressed as follows:

$$\frac{r_{ce}^2}{r_{ci}^2} = Z = const. \quad (21)$$

Some comments on the second approximation model to be noted:

1) Within the scope of the first approximation model, the radius of contact was invariable and was equal to the initial radius of physical contact r_{ci}. In comparison with the first approximation model, the real increase of the contact area (see Equation 8) affects the value R_{trm} in two ways: first, it reduces R_{max} at the expense of the radius increase in Zone 1 of the dynamic resistance curve and, second, it directly lowers the value R_{trm} at the expense of the radius increase throughout the whole welding. A registration of the radius of contact growth will allow one to normalize R_{max} and R_{trm} on the basis of the initial radius r_{ci}. From Equations 3 and 5 one can see that R_{max} and R_{trm} are inversely proportional to the contact area.

2) The second approximation model shows that the increase of the radius of contact is not accompanied by the appearance of any typical points. That is the reason that, in Zone 1 on the dynamic resistance curve its influence on the lowering of R_{max} cannot be determined by resistance variation; rather, this influence must be determined on the basis of experimental data.

3) The increase of the contact area from the beginning of the welding until the expulsion moment is described by Equation 20. The relation r_{ne}/r_{ce} depends on the welding joint size and should he specified on the basis of experimental data.

Model Correction

To correct the model, it is necessary to do the following on the basis of experimental data:

1) Find out how accurately the model enables one to determine by resistance R_{trm} the moment when the current is homogeneously distributed over the whole contact area of radius r_{ci}.

2) Define in what manner the increase of the radius of contact area during the welding process should be taken into account.

The analysis must be carried out over a wide range of welding conditions to ascertain the universality of the method. The experimental data describing resistance R_d, diameter of contact d_c, and nugget diameter d_n as a function of time was chosen. The experimental data are tabulated in Table 1 and allowed to conduct a direct test of the model. Experiments were performed for different welding conditions and were averaged over a large number of welding operations.

Let us determine how accurately the model enables one to determine by R_{trm} the moment when the current is homogeneously distributed over the whole contact area of radius r_{ci}.

Spherical-End Electrode

Consider the first welding operation in Table 1. Since the contact area increases during the welding process, one needs to know the values of the diameters of contact d_c at the moment of obtaining maximum and minimum on the curve of dynamic resistance, namely, the values d_{cRmax} and d_{ci}. This data allows one to normalize the resistance R_{max} on the basis of initial diameter d_{ci}. Taking into account the structure of Equation 3, we derive: $R'_{max} = R_{max}\,(d_{cRmax}/d_{ci})^2 = 279\ \mu\Omega$.

Substitution of R_{min} and R'_{max} into Equation 8, results in $R_{trm} = 229\ \mu\Omega$ — the predicted value of the resistance at homogeneous current distribution over the contact area of diameter d_{ci}.

Now let us compare the predicted value R_{trm} with the experimental value R_{trm}^{expr}. To reach this end, calculate on the basis of experimental data the value R_{trm}^{expr} — the resistance obtained when the current passes through the area of contact of diameter d_{ci}. Since the spherical-end electrode is used, the current is homogeneously distributed over the whole area of contact during the whole time interval soon after it attains the maximum on the dynamic resistance curve. That is why, for calculation of R_{trm}^{expr}, one

Table 1 — Experimental Data (Acceptable Nugget)

No.	Electrode Type	Thickness (mm)	Welding Current (A)	Welding Time (c)	Force (kg)	d_{ci} (mm)	d_{cRmax} (mm)	d_{ce} (mm)	R_{min} (μΩ)	R_{max} (μΩ)	R_d (μΩ)	Ref.
1	Sph. 30 mm R	0.8	6,000	15	120	2.90	3.35	4.40	165	209	120	2
2	Sph.100 mm R	0.8	6,000	15	120	3.20	3.75	4.90	163	188	121	2
3	Sph. 30 mm R	0.8	12,000	15	400	3.80	4.50	7.20	87	116	52	2
4	Sph.100 mm R	0.8	12,000	15	400	5.00	5.60	7.20	86	99	58	2
5	Flat 4.8 mm	0.8	6,000	15	190	4.10	4.80	5.70	111	129	92	2
6	Flat 6.8 mm	0.8	12,000	15	380	5.00	5.80	7.00	80	86	56	2

can use the values d_c and R_d in any point of the indicated time interval. It is most interesting to use the data related to the very end of the welding process, *i.e.*, d_{ce} and R_{de}, respectively. Taking into account that current is homogeneously distributed over the whole area of contact, we derive: $R_{trm}^{expr} = R_{de}(d_{ce}/d_{ci})^2 = 276\ \mu\Omega$.

Similarly, on the basis of data No. 2 through No. 4 in Table 1, the values R_{trm}^{expr} and R_{trm} are obtained. All of them are tabulated in Table 2.

Experimental material related to the welding operations performed with the expulsion (Table 3) provides the opportunity to directly test Equation 20. For example, data No. 1 and No. 2 in Table 3 show deviations of no more than 10%.

Equation 20 admits expulsion not only at the late stages of welding process, but also at the earlier stages of the process when the nugget diameter is still relatively small. Such occurrence actually takes place (see Table 3, No. 3). Suhstitution of these values in Equation 20 shows that they conform to the expulsion condition. A similar case is described in Ref. 3 and arises at relatively large welding currents.

The analysis of welding operations carried out in a wide range of condition variations, such as electrode force, welding current, welding time and electrode geometry, enables one to consider the effect of different factors in the following manner:

1) The increase of the diameter of contact from d_{ci} to d_{cRmax} can be taken into account by calculating the relation d_{cRmax}/d_{ci}, which varies slightly with the change of the welding conditions (by no more than 3% of the mean value) and is equal to 1.16. This is the reason for the substitution in Equation 8 of the value $(1.16)^2 R_{max} = 1.35\ R_{max} = X\ R_{max}$ instead of R_{max}.

2) In comparison with the experimental data, the model gives the underestimated values of resistance R_{trm}. The mean deviation value is 23%, and its

Table 2 — R_{trm} (Predicted and Experimental)

No.	R_{trm} (μΩ)	R_{trm}^{expr}
1	229	276
2	204	283
3	137	186
4	96	120
5	142	178
6	90	110

scattering under the changes of the welding conditions does not exceed 5%. Most likely, such lowered resistance value is explained by the fact that at the moment of attaining R_{max} the deviation upwards occurs from the flat peak in the curve of current density distribution. This deviation is connected with the finite thickness of workpieces. Besides, the metal heating degree is still not very large, so the current density J_u, which is considered as a constant value throughout the whole welding, is somewhat greater than it really is during the current termination. Thus the value R_{trm} in Equation 8 must be increased by $1/(1-0.23) = 1.3 = Y$ times.

3) The relation $(d_{ce}/d_{ci})^2 = Z$ depends on dimensions of weld joint.

Consideration of the above listed factors results in the following equation for calculating the optimal value of resistance R_{opt}:

$$R_{opt} = \frac{YR_{min}}{2Z\left(1-\sqrt{1-\frac{R_{min}}{XR_{max}}}\right)} = \frac{R_Z}{Z}. \qquad (22)$$

Equation 22 describes a desired algorithm of adaptive control system operation. Parameters X and Y do not depend on the welding conditions. Parameter Z depends on the weld joint dimensions.

Flat-End Electrode

One calculates the values R_{trm} and R_{trm}^{expr} in the same manner as it was performed for the spherical-end electrode. These values are tabulated in Table 2, on the basis of data No. 5 and No. 6 in Table 1. Now it is possible to define parameters X, Y and Z. We have obtained the following magnitudes: X = 1.35, Y = 1.24 and Z = 1.94. Change of electrode geometry results, on one hand, in a variation of parameters Y and Z, and, on the other hand, in almost complete independence of parameter Z from the weld joint dimensions. The value Z, obtained for workpieces with small thicknesses, also remains the same for thicknesses up to 8.0 mm.

The experimental test of the synthesized method efficiency should be the final stage.

Experimental Test

The efficiency test for the synthesized method is conducted on the basis of experimental data. This test should be performed in cases of deviations from optimal values of such principal parameters as welding current, welding time, electrode force, and electrode geometric dimensions. As previously mentioned, experimental data describing resistance and nugget diameter as a function of time were chosen (Refs. 2–4). Experiments were performed for different welding conditions and were averaged over a large number of welding operations.

Spherical-End Electrode

To calculate R_{opt} according to Equation 22, it is essential to know parameter Z, which can be determined by Equation 20. However, this method requires laboratory research to define the values r_{ne} and r_{ce}. It is easier to determine Z by carrying out the basic welding in which the nugget size will be close to the maximum possible under the given conditions (the state close to expulsion). For the basic welding, the values of R^B_{min} and R^B_{max} allow one to calculate R^B_Z. Resistance at the moment of current termination R^B_e may be considered equal to R^B_{opt}. Then

Table 3 — Experimental Data (Expulsion)

No.	Electrode Type	Sheet Thickness (mm)	Welding Current (A)	Welding Time (c)	Force (kg)	d_{cl} (mm)	d_{ne} (mm)	d_{ce} (mm)	Ref.
1	Sph. 50 mm R	0.8	8,000	12	175	3.30	5.10	5.60	4
2	Sph. 50 mm R	0.8	8,000	12	175	3.20	4.90	5.40	4
3	Sph. 50 mm R	0.8	8,000	12	175	3.20	4.10	4.80	4

the value Z can be determined by Equation 22. Perform the test of the control system operation by comparing the welding operations, assuming one of them is the basic one. Then, when carrying out any other welding operation, the control system will terminate the welding process when reaching $R_{opt} = R^B_{opt} (R_Z/R^B_Z)$.

We will discuss the control system operation under the conditions of welding current change on the basis of experimental data obtained by Nakata (Ref. 2) and Cho (Ref. 5). It is seen from literature data that, when the welding current changes over a wide range, the values R_{min} and R_{max} vary in such a way that the calculated value R_Z alters only insignificantly. In this case, the control system will keep the value R_{opt} constant. For the spherical-end electrode it means that the diameter of contact d_{ce} is also constant. Using this, we will consider two welding operations performed by Nishiguchi (Ref. 4) for the workpieces with a thickness of 0.8 mm. Assume the first of these operations is the basic one.

1) El type — 50R; I = 6000 A; t = 12 c; F = 175 kg; d_{ce} = 4.6 mm; d_n = 3.95 mm.

2) El type — 50R; I = 8000 A; t = 4 c; F = 175 kg; d_{ce} = 4.6 mm; d_n = 3.90 mm.

In the considered example, as the welding current I increased from 6000 A to 8000 A, the control system kept the value d_{ce} constant and reduced the welding time from 12 to 4 cycles. The nugget diameter did not change.

Examine the control system operation under the conditions of electrode force changing, remembering that considerable force variations cannot be balanced simply by welding time change; therefore, the welding current should also be changed simultaneously with the force alteration. As an example, consider two welding operations (see No. 2 and No. 4 in Table 1). By Equation 22, the values R_{Z2} and R_{Z4} are calculated: R_{Z2} = 203 μΩ; R_{Z4} = 106 μΩ. Assume that the welding operation No. 2 is the basic one. When performing the basic welding operation, the nugget diameter constituted 4.1 mm. For the welding process No. 4, $R_{opt4} = R_{opt2} (R_{Z4}/R_{Z2})$ = 63 μΩ is obtained. By the moment of attaining this value, the weld duration made up 12 cycles and the nugget had the diameter d_n = 6.4 mm.

We will discuss the control system operation under the conditions of electrode tip mushrooming on the basis of the material obtained by Nakata (Ref. 3), which presents data on the welding operations performed without the replacement of the electrode tips. Assume that the first of these operations (30th spot) is the basic one, and consider the control system behavior when operating with complete tip mushrooming (4245th spot):

1) Weld No. 30; t = 24 c; R_{min} = 209 μΩ; R_{max} = 212 μΩ; $R_{opt} = R_{de}$ = 171μΩ; d_n = 6.0 mm.

2) Weld No. 4245; R_{min} = 195 μΩ; R_{max} = 196 μΩ.

On the basis of this data R_{Z1} = 217 μΩ; R_{Z2} = 200 μΩ; then $R_{opt2} = R_{opt1} (R_{Z2}/R_{Z1})$ = 157 μΩ.

By the moment of reaching this value, the welding duration made up t = 22 cycles, and the nugget diameter d_n = 6.04 mm.

Flat-End Electrode

In the case of the flat-end electrode, the basic welding is not required because the parameters X, Y, and Z are determined in advance. Let us illustrate the control system operation under the conditions of the alteration both of the welding current and of the electrode force using welds No. 5 and No. 6 in Table 1. The values R_{opt5} and R_{opt6} are calculated on the basis of Equation 22, R_{opt5} = 89 μΩ; R_{opt6} = 58 μΩ. In the first case the weld time t = 17 c, and the nugget diameter d_n = 5.6 mm. In the second case: t = 14 c, d_n = 7.0 mm.

We will use the obtained method for the workpieces with thicknesses 1.6 mm on the basis of the material obtained by Cho (Ref. 5). The weld operation was carried out at the current I = 6900 A. The following parameters were obtained: R_{min} = 113 μΩ and R_{max} = 158 μΩ. The calculated resistance R_{opt} = 115 μΩ. By the moment this value was achieved, t = 20 c and d_n correspond to the welding process performed with the expulsion.

Let us illustrate universality of the method on the basis of the data obtained by Gedeon, *et al.* (Ref.1). The authors give us the dynamic resistance curve of a good weld. It is also known that the flat-end electrode was used. There is no information about thickness of workpieces, electrode diameter and electrode force. The following parameters were obtained: R_{min} = 83 μΩ and R_{max} = 132 μΩ. The calculated resistance R_{opt} = 98 μΩ. The calculated resistance (98 μΩ) is very close to the resistance at the very end of the weld cycle (95 μΩ) . It is important that the welding time for this particular weld (24 c) is almost twice as long as the welding time for the welding operations we used for the model correction.

Conclusion

The universal method for assuring the quality and consistency of resistance spot welds in uncoated steel sheet was developed. The method is based on dynamic resistance and allows us to predict the moment of current termination for different welding conditions and different electrode configurations. The method discussed uses the dynamic resistance curve and does not require specific information about welding conditions.

Validation of the method has been confirmed experimentally. The comparison of results shows that the method provides the maximum nugget size with an alteration of welding time, welding current, and electrode force. The change of geometry of electrode tips up to and including complete tip mushrooming is compensated by utilizing this method.

When applying this method in industrial conditions, when the welding time must be constant, it is advisable to compensate for the existing deviations in welding conditions by altering the welding current; thus, supply the control system with a resistance weld controller (Refs. 12, 13). In this case, the current value will indirectly reflect the nugget size and the electrode tip mushrooming.

Further work is needed to create a

method that can be applied to coated materials and high-strength low-alloy steel.

Appendix

Linear Combination of Two Different Types of the Current Density Distributions: an Explanation

To prove that Equation 8 is the desired algorithm of the adaptive control system functioning within the scope of the first approximation model, we shall derive Equations 6 and 7. To reach this end, let us introduce a new condition:

$$\frac{J_{usp}}{K_1 J_m} = \frac{J_{ufl}}{K_2 J_m} = Q.$$

Let us define the current I_{Rmin}, passing through the whole contact area at the moment when the minimum on the dynamic resistance curve is reached. It follows from Equations 2 ,10, and 13 that I_{Rmin} may be written as:

$$I_{Rmin} = \frac{\pi \cdot K_1 J_m r_{ci}^2}{2} + \frac{\pi \cdot K_2 J_m r_{ci}^2}{2}$$

$$= \frac{\pi \cdot J_m r_{ci}^2}{2}(K_1 + K_2).$$

Let us similarly define the current I_{Rmax}, passing through the whole contact area at the moment when the resistance reaches its maximum. It follows from Equations 3 ,11, and 13 that I_{Rmax} may be written as:

$$I_{Rmax} = \frac{\pi \cdot K_1 J_m r_{ci}^2}{2}\left[1-\left(1-\frac{J_{usp}}{K_1 J_m}\right)^2\right]$$

$$+\frac{\pi \cdot K_2 J_m r_{ci}^2}{2}\left[1-\left(1-\frac{J_{ufl}}{K_2 J_m}\right)^2\right]$$

$$= \frac{\pi J_m r_{ci}^2}{2}(K_1 + K_2)\cdot\left[1-(1-Q)\right].$$

Finally, let us define the current I_{trm} at the moment of the current termination. It follows from Equations 5 ,12, and 13 that I_{trm} may be expressed as:

$$I_{trm} = pJ_{usp} r_{ci}^2 + pJ_{ufl} r_{ci}^2$$
$$= pr_{ci}^2\left(J_{usp} + J_{ufl}\right)$$

Taking into account the new condition $J_{usp}/K_1 J_m = J_{ufl}/K_2 J_m = Q$, the last equation may be rewritten as:

$$I_{trm} = \pi \cdot r_{ci}^2\left(J_{usp} + J_{ufl}\right)$$

$$= \pi \cdot r_{ci}^2\left(QK_1 J_m + QK_2 J_m\right)$$

$$= \pi r_{ci}^2 J_m Q \cdot (K_1 + K_2).$$

It is easy to see, that the equations for the currents I_{Rmin}, I_{Rmax}, and I_{trm} are similar to Equations 2, 3, and 5, respectively. Therefore, Equation 6 and Equation 7 take place and resistance R_{trm} is determined by Equation 8. It should be noted again that Equation 8 takes place only if condition $J_{usp}/K_1 J_m = J_{ufl}/K_{2m} = Q$ is satisfied.

Depending on the value of Q, we will consider three different types of current density distribution when the maximum resistance on the dynamic resistance curve is achieved. Type 1, Type 2 and Type 3 correspond to $Q > 0.5$, $Q = 0.5$ and $Q < 0.5$, respectively. For example, let us consider the current density distribution when $K_1/K_2 = 3$. Figures 6A–C illustrate the current density distribution for $Q = 0.7$ (Type 1), $Q = 0.5$ (Type 2), and $Q = 0.3$ (Type 3), respectively. At the moment when the maximum resistance on the dynamic resistance curve is achieved, one can find four different regions on the current density distribution curve:

$J(r) = J_{usp}(r) + J_{ufl}(r)$ (Region 1)
$J(r) = J_{usp}(r) + K_2 J_{fl}(r)$ (Region 2)
$J(r) = J_{ufl}(r) + K_1 J_{sp}(r)$ (Region 3)
$J(r) = K_1 J_{sp}(r) + K_2 J_{fl}(r)$ (Region 4)

If $Q > 0.5$, Regions 2, 3, and 4 are presented on the current density distribution curve (Fig. 6A). If $Q < 0.5$, Regions 1, 2, and 3 are presented on the current density distribution curve (Fig. 6C). If $Q = 0.5$, only Regions 2, and 3 are presented on the current density distribution curve (Fig. 6B). The central zone (Region 2) has a smaller value of current density. At the late stages of welding process, Region 2 will be replaced with Region 1, having greater current density value. Within the scope of the first approximation model, this corresponds to the indentation of the electrode tips into the material and a reduction of the current path in Zone 3 of the dynamic resistance curve.

References

1. Gedeon, S. A., Sorensen, C. D., Ulrich, K.T., and Eagar, T. W. 1987. Measurement of dynamic electrical and mechanical properties of resistance spot welds. *Welding Journal* 66(12): 378-s to 385-s.

2. Nakata, S., Nishimura, A., Otani, T., and Tamada, O. 1982. Significance of resistance and voltage between electrode tips and proposal of new adaptive control system for quality assurance. IIW Doc. III- 718-82, International Institute of Welding.

3. Nakata, S., Aono, K., Suzuki, N., Kawaguchi, Y., and Inoue, M. 1982. Quality assurance characteristics in resistance spot welds by adaptive control system and its field applications. IIW Doc. III-720-82, International Institute of Welding.

4. Nishiguchi, K., and Matsuyama, K. 1987. Influence of current wave form on nugget phenomena when spot welding thin steel sheet. *Welding in the World* 25 (11/12): 222–244.

5. Cho, H., and Cho, Y. 1985. A theoretical model for dynamic resistance spot welds. Proceedings of Institution of Mechanical Engineers, Vol. 199, No. B2, pp. 71–79.

6. Dickinson, D. W., Franklin, J. E., and Stanya, A. 1980. Characterization of spot welding behavior by dynamic electrical parameter monitoring. *Welding Journal* 59(6): 170-s to 176-s.

7. Nied, H. A. 1984. The finite element modeling of the resistance spot welding process. *Welding Journal* 63(4): 123-s to 132-s.

8. Bowers, R. J., Sorensen, C. D., and Eagar, T. W. 1990. Electrode geometry in resistance spot welding. *Welding Journal* 69 (2): 45-s to 51-s.

9. Hawkins, I. Superior quality production spot welding using adaptive control. IIW Doc. III-820-85, International Institute of Welding.

10. Dzuranyi, E., Janota, M., Kuhan, J. VUZ — Autoset-R Automatic control system of resistance spot welding. IIW Doc. No. IIIG-75-81, International Institute of Welding.

11. Bhattacharya, S., and Andrews, D. R. 1974. Significance of dynamic resistance curves in the theory and practice of spot welding. *Welding and Metal Fabrication* 9: 296–301.

12. Cullison, A. 1993. Resistance weld controller delivers the heat where it's needed. *Welding Journal* 72(6): 47–49.

13. Livshits, A. G., and Shereverov, V. I. 1993. Optimal resistance weld controller for single-phase welding machines. *Electrical Engineering* 3: 39–41.